International Research Journal of Innovations in Engineering and Technology (IRJIET)

ISSN (online): 2581-3048
Volume 10, Issue 6, pp 266-276, June-2026
https://doi.org/10.47001/IRJIET/2026.106034

Design Methodology of a Dual-Medium Propeller Using BET

[1]Hritika Chafekar, [2]Prasad Gonewar, [3]Karan Kunte, [4]Dheeraj Kamble, [5]Dr. Sunil Patil

[1,2,3,4,5]Department of Mechanical Engineering, All India Shri Shivaji Memorial Society's College of Engineering, Pune, Maharashtra, India

***Abstract* - Hybrid aerial-underwater vehicles (HAUVs) require propulsion systems capable of operating efficiently in two fluids with significantly different physical properties. Conventional solutions typically employ separate propulsion systems for aerial and underwater operation, increasing system complexity, weight, and power consumption. This work presents the design methodology and numerical investigation of a dual-medium propeller intended for operation in both air and water. The propeller geometry was developed using Blade Element Theory (BET) combined with aerofoil performance data obtained from the NACA 4412 profile. Analytical predictions of thrust and torque were used to establish the blade chord and twist distributions, while computational fluid dynamics (CFD) simulations were performed to assess the aerodynamic and hydrodynamic behaviour of the final geometry.**

A steady Reynolds-Averaged Navier–Stokes (RANS) formulation with the SST k–ω turbulence model was employed to evaluate propeller performance in both operating media. Structural calculations were conducted to provide a first-order assessment of bending, torsional, and centrifugal stresses acting on the blade. Results indicate that the proposed design methodology produces a propeller capable of generating useful thrust in both air and water while maintaining acceptable preliminary structural integrity. The study establishes a framework for dual medium propeller development and provides a foundation for future experimental validation and optimisation.

Keywords: Dual-medium propeller, hybrid aerial underwater vehicle, Blade Element Theory, computational fluid dynamics, NACA 4412, propeller design.

I. INTRODUCTION

Hybrid aerial–underwater vehicles (HAUVs) have emerged as a promising class of unmanned systems capable of operating in both atmospheric and aquatic environments. Such vehicles combine the rapid deployment capability of unmanned aerial vehicles (UAVs) with the exploration and inspection capabilities of underwater robotic platforms. Potential applications include environmental monitoring, defence reconnaissance, offshore inspection, search-and-rescue operations, and scientific data collection.

Despite their advantages, the development of efficient HAUVs remains challenging due to the substantial differences between air and water. Water possesses a density approximately 800 times greater than air and exhibits significantly different flow behaviour [1]. Consequently, propulsion systems designed for aerial applications often perform poorly underwater, while marine propellers generally fail to provide sufficient efficiency for flight.

Many existing HAUV designs employ separate propulsion systems for each operating environment. Although effective, this approach introduces additional mass, increases mechanical complexity, and reduces overall system efficiency. Modern operational cross-domain platforms require highly specialized, streamlined configurations to handle fluid transition mechanics [2], [3]. A dual-medium propeller capable of operating in both fluids offers a potential solution by reducing component count and simplifying vehicle architecture.

Designing such a propeller is a multidisciplinary challenge involving aerodynamic performance, hydrodynamic performance, structural integrity, manufacturability, and operational robustness. In particular, the blade geometry must provide acceptable performance over a wide range of operating conditions while remaining structurally capable of withstanding the substantially higher loads encountered underwater. The objective of the present work is to establish a systematic design methodology for a dual-medium propeller using analytical and numerical techniques. Blade Element Theory (BET) is employed to generate an initial blade geometry, while computational fluid dynamics (CFD) is used to assess flow behaviour and performance trends. The resulting methodology is intended to provide a foundation for future optimisation and experimental validation.

© 2026 IRJIET All Rights Reserved

International Research Journal of Innovations in Engineering and Technology (IRJIET)

ISSN (online): 2581-3048

Volume 10, Issue 6, pp 266-276, June-2026

https://doi.org/10.47001/IRJIET/2026.106034

II. LITERATURE REVIEW

The design of propellers has historically been based on the concept of a rotating wing, where each radial section of a blade generates aerodynamic forces that collectively produce thrust and torque [4]. Blade Element Theory (BET) and Blade Element Momentum Theory (BEMT) remain widely used tools for preliminary propeller design due to their computational efficiency and physical insight. While analytical approaches are useful during the early stages of development, they cannot fully capture complex three-dimensional flow structures such as tip vortices, wake interaction, and rotational effects. Consequently, computational fluid dynamics (CFD) has become an essential component of modern propeller design and verification.

Recent research in dual-medium propulsion has highlighted the challenges associated with operating a single propeller in both air and water. Investigations involving conventional aerial propellers have shown that underwater operation can result in excessive torque requirements and reduced efficiency. Other researchers have explored adaptive and morphing propeller concepts [5]; however, these solutions often increase mechanical complexity and manufacturing cost.

Advances in numerical optimisation techniques have enabled the development of dedicated amphibious propellers through the simultaneous optimisation of blade planform geometry, twist distribution, and aerofoil shape. These studies have demonstrated measurable improvements in underwater efficiency while maintaining acceptable aerial performance [6]. Recent vehicle-level deployments, such as fixed-wing and multirotor trans-media sub-aerial drones, highlight the acute need for rigid, high-stiffness geometric designs that do not experience drastic structural degradation under dual loading regimes [7], [8].

The literature indicates that successful dual-medium propeller development requires:

- Appropriate aerofoil selection.
- Careful optimisation of chord and twist distributions.
- Numerical verification using CFD.
- Structural assessment under combined loading.
- Experimental validation under realistic operating conditions.

The present study builds upon these principles by integrating analytical design, CFD assessment, and structural evaluation within a unified development framework.

III. OBJECTIVES

The objectives of this work are:

1) To employ a systematic design methodology for a dual medium propeller capable of operating in both air and water.
2) To establish blade geometry parameters using Blade Element Theory and aerofoil performance characteristics.
3) To evaluate propeller performance through numerical simulations and analytical calculations.
4) To assess structural integrity under aerodynamic and hydrodynamic loading conditions.
5) To identify design factors influencing performance, efficiency, and structural behaviour.

IV. METHODOLOGY

The overall design methodology adopted in this study is illustrated in Fig. 1.

The development procedure consisted of five major stages:

1) Aerofoil selection.
2) Blade geometry generation using Blade Element Theory.
3) Three-dimensional CAD modelling.
4) Numerical assessment using CFD.
5) Structural evaluation and performance assessment.

Initially, candidate aerofoils were reviewed based on their lift-to-drag characteristics within the Reynolds number range relevant to both aerial and aquatic operation. The NACA 4412 aerofoil was selected owing to its favourable performance characteristics and extensive availability of published aerodynamic data.

Using the selected aerofoil, blade chord and twist distributions were generated through Blade Element Theory calculations. The resulting geometry was subsequently modelled in a three-dimensional CAD environment.

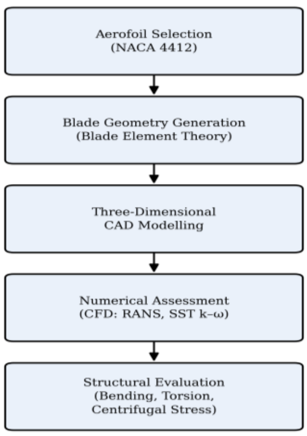

Figure 1: Overall design methodology adopted for the dual-medium propeller development Process

Initially, candidate aerofoils were reviewed based on their lift-to-drag characteristics within the Reynolds number range

International Research Journal of Innovations in Engineering and Technology (IRJIET)

ISSN (online): 2581-3048

Volume 10, Issue 6, pp 266-276, June-2026

https://doi.org/10.47001/IRJIET/2026.106034

relevant to both aerial and aquatic operation. The NACA 4412 aerofoil was selected owing to its favourable performance characteristics and extensive availability of published aerodynamic data.

Using the selected aerofoil, blade chord and twist distributions were generated through Blade Element Theory The resulting geometry was subsequently modelled in a three-dimensional CAD environment.

CFD simulations were then conducted to evaluate flow behaviour, thrust generation, torque requirements, and pressure distributions in both operating media. Finally, analytical structural calculations were performed to estimate stresses and blade deformation under representative operating loads.

V. AEROFOIL SELECTION

The NACA 4412 aerofoil was selected as the baseline profile for the propeller blade. This aerofoil is characterised by a maximum camber of 4% located at 40% chord and a maximum thickness of 12% of the chord length.

The selection was based on the following considerations:

- Good lift-to-drag ratio at low and moderate Reynolds numbers.
- Smooth stall characteristics.
- Extensive availability of experimental and numerical data.
- Proven performance in propeller and low-speed aerodynamic applications.

The operational angle-of-attack range was selected based on published aerofoil performance data and numerical assessment. While specialized profiles exist for distinct media, the NACA 4412 was selected as an intentional geometric compromise to establish a functional, baseline performance envelope across both fluids without requiring complex mechanical morphing systems. The design objective was to maintain blade sections near the region of maximum lift-to-drag ratio while avoiding excessive drag penalties and flow separation.

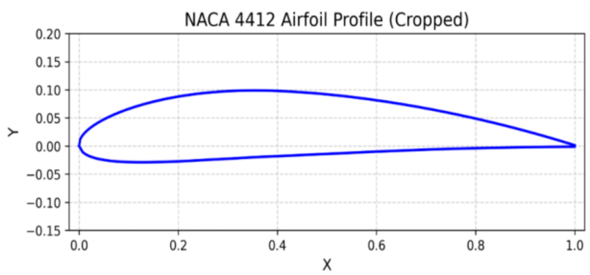

Figure 2: NACA 4412 aerofoil used for blade development

VI. AERODYNAMIC AND HYDRODYNAMIC CONSIDERATIONS

The flow behaviour around the blade is governed by the Reynolds number:

$$Re = \frac{\rho V c}{\mu} \quad \ldots\ldots\ldots\ldots\ldots\ldots\ldots\ldots (1)$$

where ρ is fluid density, V is local velocity, c is aerofoil chord length, and μ is dynamic viscosity.

The large difference in density between air and water results in significantly different loading conditions for the same blade geometry. Consequently, the design process must balance aerodynamic efficiency with structural robustness.

VII. PROPELLER DESIGN USING BLADE ELEMENTTHEORY

Blade Element Theory (BET) was employed to generate the initial propeller geometry. In this approach, the blade is divided into a number of radial sections, each of which is analysed independently. The local aerodynamic forces acting on each blade element are subsequently integrated along the span to obtain the total thrust and torque.

7.1 Design Requirements

The propeller architecture was designed to satisfy the performance envelopes of two entirely distinct operational regimes dictated by fluid properties: a high-speed aerial cruise phase running at 8000 RPM to actively compensate for low atmospheric density, and a submerged aquatic phase restricted to 1200 RPM. While multi-medium physical switchover states rely on a dedicated electronic variable-speed motor controller system, the baseline geometric design properties are detailed in Table 1.

Table 1: Design Parameters

Parameter	Value
Propeller diameter (m)	0.20
Propeller radius (m)	0.10
Hub radius (m)	0.02
Blade length (m)	0.08
Number of blades	4
Base rotational speed (RPM) (water)	1200
Base rotational speed (RPM) (air)	8000
Design fluid density (water) (kg/m^3)	1000
Design fluid density (water) (kg/m^3)	1.225

7.2 Blade Element Formulation

For each blade element, the differential lift (dL) and drag (dD) forces are expressed as:

© 2026 IRJIET All Rights Reserved

International Research Journal of Innovations in Engineering and Technology (IRJIET)

ISSN (online): 2581-3048

Volume 10, Issue 6, pp 266-276, June-2026

https://doi.org/10.47001/IRJIET/2026.106034

$$dL = \frac{1}{2}\rho V^2 {}_{c}C_{d}\, dr \ldots\ldots\ldots\ldots\ldots(2)$$

$$dL = \frac{1}{2}\rho V^2 {}_{c}C_{l}\, dr \ldots\ldots\ldots\ldots\ldots(3)$$

where ρ is the fluid density, V is the local flow velocity, c is the local chord length, C_l is the lift coefficient, C_d is the drag coefficient, and dr is the radial element width.

To aggregate these elemental contributions across a propeller featuring a total number of blades B, the total integrated thrust (T) and torque (Q) are established mathematically using the local inflow angle ϕ via:

$$T = B\int_{Rhub}^{Rtip}(dL\cos\phi - dD\sin\phi) \ldots\ldots\ldots\ldots\ldots(4)$$

$$Q = B\int_{Rhub}^{Rhub}(dL\sin\phi + dD\cos\phi)r dr \ldots\ldots\ldots\ldots(5)$$

These classic integral transformations map directly back to foundational lifting-line and distributed element aerodynamic theories detailed by Glauert [9] and Leishman [10]. The thrust and torque contributions from each element were calculated and integrated across the blade span.

7.3 Blade Geometry Development

The final geometry was developed through multiple design iterations. The chord distribution and twist angle were adjusted to maintain operation near the desired angle of attack over the entire blade span.

The final design incorporated approximately 35◦ of root twist, a refined chord distribution, and moderate blade skew to improve load distribution and operational stability.

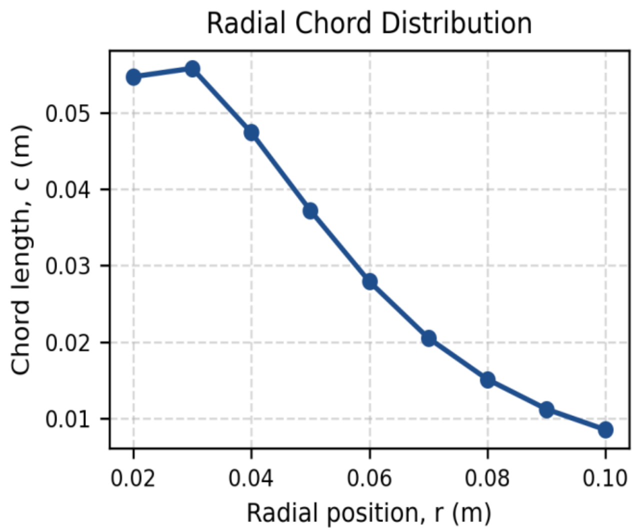

Figure 3: Radial chord distribution used in the final propeller design

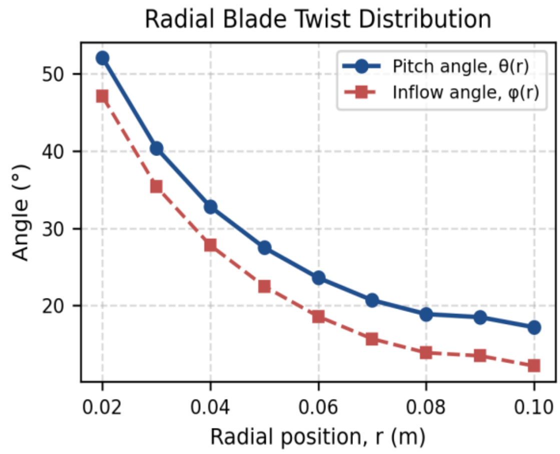

Figure 4: Blade twist distribution along the span

VIII. CAD DEVELOPMENT

Following analytical design, the propeller geometry was generated using a three-dimensional CAD environment.

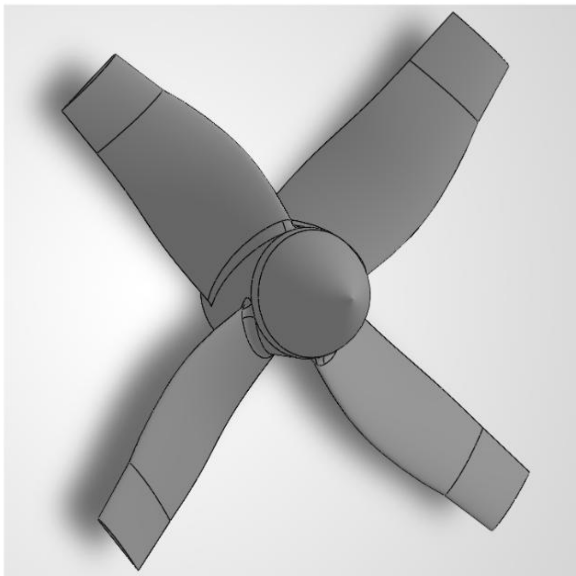

Figure 5: Initial propeller geometry

The propeller geometry was refined through three major design iterations, each evaluated against CFD before proceeding to the next.

The baseline geometrya flat, untwisted four-blade propeller was first evaluated at an aerial cruise condition of 25 m/s at 8000 RPM (J ≈ 0.93) and an aquatic condition of 4 m/s at 1200 RPM (J ≈ 1.0). At these operating points, CFD predicted thrust values 66.3% (air) and 64.5% (water) below the BET estimate. This shortfall was attributed to the advance ratio exceeding approximately 0.9, a regime in which forward velocity dominates over rotational velocity, causing the local blade angle of attack and consequently lift and thrust to collapse.

© 2026 IRJIET All Rights Reserved

International Research Journal of Innovations in Engineering and Technology (IRJIET)

ISSN (online): 2581-3048

Volume 10, Issue 6, pp 266-276, June-2026

https://doi.org/10.47001/IRJIET/2026.106034

To isolate the contribution of advance ratio from that of blade geometry, the second iteration held the blade shape fixed and instead revised the target cruise condition to 18 m/s (air) and 3 m/s (water) at unchanged rotational speeds, bringing the advance ratio to 0.675 and 0.75 respectively within the 0.6–0.9 band identified as favourable. This single change reduced the CFD–BET thrust discrepancy to 51% (air) and 47.5% (water) and raised efficiency from 62% to 78.2% (air) and from 67% to 83.6% (water), confirming that advance ratio accounted for a substantial but not complete share of the original performance gap.

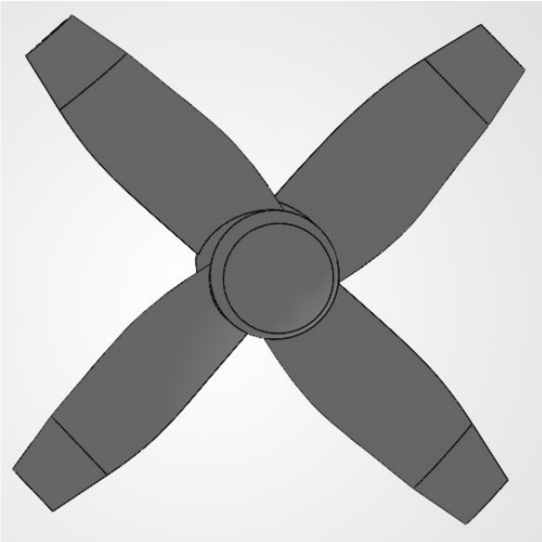

Figure 6: Intermediate optimized geometry

With the advance ratio fixed at approximately 0.675, the third iteration addressed the remaining discrepancy through blade geometry alone. The chord distribution was re-derived using elliptical loading theory, and a 35° root twist with a 20° blade skew were introduced to improve spanwise load distribution.

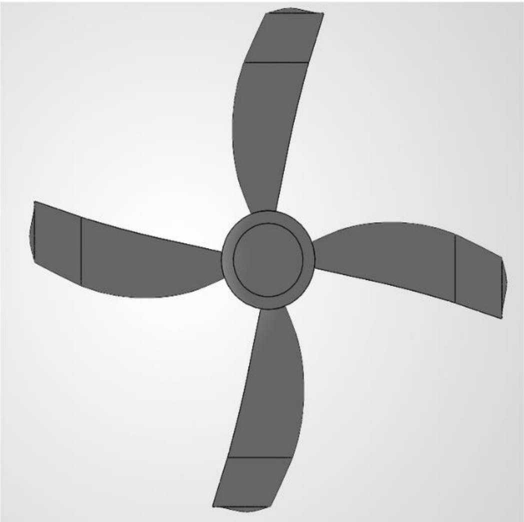

Figure 7: Final optimized dual-medium propeller geometry

Propeller diameter, blade count, and hub radius were held constant across all three iterations. This geometric refinement closed the remaining gap, reducing the thrust discrepancy to 23.4% in air and effectively eliminating it in water, where the CFD result (296.70 N) marginally exceeded the BET prediction (293.46 N) the values reported in Table 2.

With the advance ratio fixed at approximately 0.675, the third iteration addressed the remaining discrepancy through blade geometry alone. The chord distribution was re-derived using elliptical loading theory, and a 35° root twist with a 20° blade skew were introduced to improve spanwise load distribution. Propeller diameter, blade count, and hub radius were held constant across all three iterations. This geometric refinement closed the remaining gap, reducing the thrust discrepancy to 23.4% in air and effectively eliminating it in water, where the CFD result (296.70 N) marginally exceeded the BET prediction (293.46 N) the values reported in Table 2.

IX. COMPUTATIONAL FLUID DYNAMICS METHODOLOGY

Computational Fluid Dynamics (CFD) simulations were conducted to assess aerodynamic and hydrodynamic performance.

9.1 Aerofoil Simulations

Two-dimensional simulations were performed to evaluate the selected aerofoil over a range of operating angles of attack. The numerical setup consisted of:

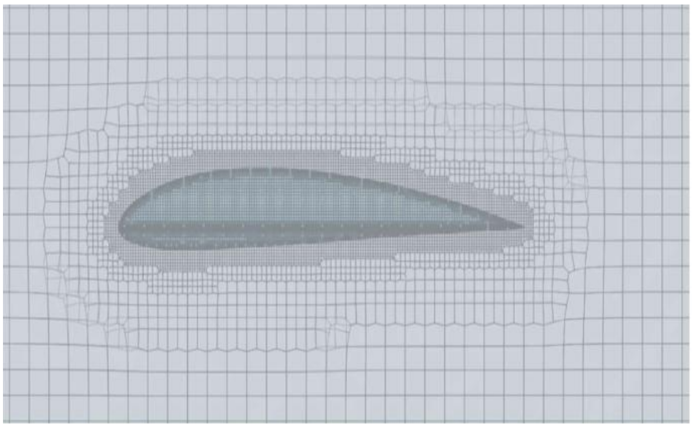

Figure 8: Mesh for aerofoil simulation in water

- Steady incompressible RANS formulation.
- SST k–ω turbulence model.
- Structured mesh with inflation layers to achieve proper boundary layer refinement.
- Velocity inlet boundary condition.
- Pressure outlet boundary condition.
- No-slip aerofoil surface.

© 2026 IRJIET All Rights Reserved

International Research Journal of Innovations in Engineering and Technology (IRJIET)

ISSN (online): 2581-3048

Volume 10, Issue 6, pp 266-276, June-2026

https://doi.org/10.47001/IRJIET/2026.106034

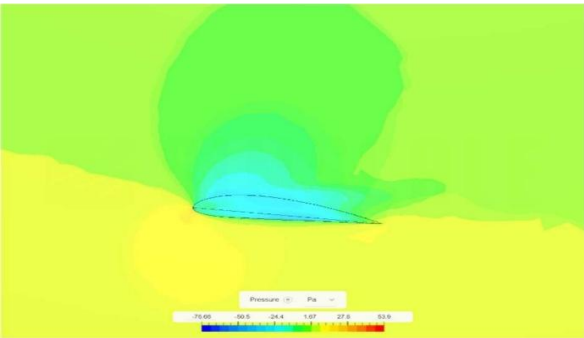

Figure 9: Representative static-pressure contour around the NACA 4412 aerofoil section at the design angle of attack

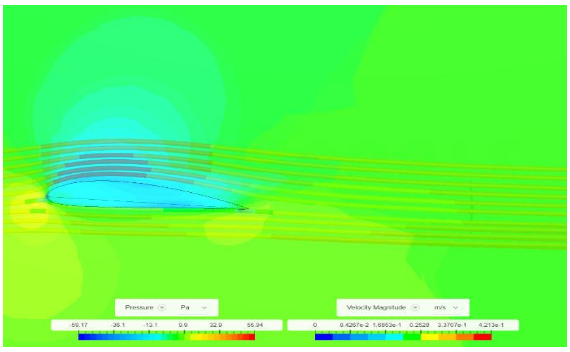

Figure 10: Representative velocity contour around the NACA 4412 aerofoil section at the design angle of attack

9.2 Propeller Simulations

Three-dimensional propeller simulations were performed using a Moving Reference Frame (MRF) approach. To resolve peak operational forces under conservative loading envelopes, all simulations were executed under static (zero-forward velocity/bollard pull) conditions. Prior to compiling final production outputs, a rigorous grid independence check was executed across three varying mesh levels (4.3M, 6.8M, and 15.2M volume elements), as shown in Fig. 11.

The intermediate 6.8M element hex-dominant mesh configuration was ultimately selected for all subsequent design runs as it demonstrated a strict performance convergence with an observed thrust variance of approximately 1.4% relative to the finest localized grid.

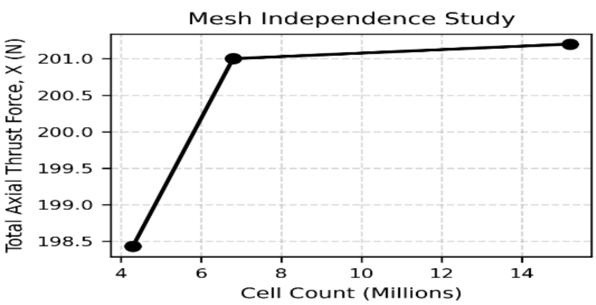

Figure 11: Mesh independence study: variation of total axial thrust force with cell count for the water operating condition

Representative iterative convergence histories of the total force and moment monitors for the selected mesh confirmed that a stable steady-state solution was reached well within the simulated time window for both the water and air operating conditions.

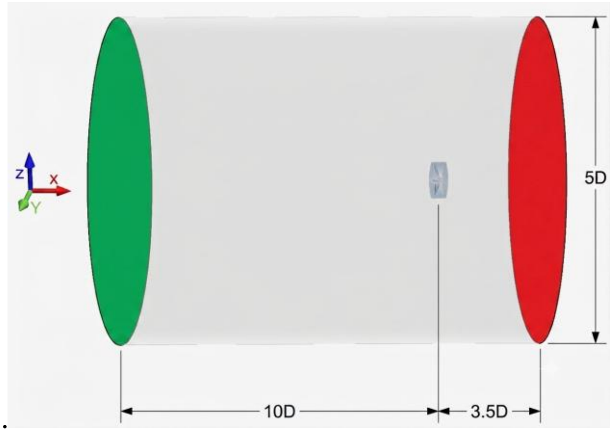

Figure 12: CFD computational domain and rotating region

The computational domain consisted of:

- Cylindrical outer domain.
- Rotating inner fluid zone.
- Stationary outer fluid region.
- Hex-dominant volume mesh.

The SST k–ω turbulence model was selected owing to its capability to accurately predict boundary-layer behaviour, shear flow propagation, and adverse pressure-gradient effects commonly encountered in highly loaded propeller wakes, as extensively validated by Menter [12].

The steady-state MRF formulation used here serves as an established, computationally efficient alternative to fully transient sliding mesh structures for bollard-pull characterization [13].

X. RESULTS AND PERFORMANCE ASSESSMENT

10.1 Aerofoil Performance

The aerofoil simulations demonstrated a generally linear increase in lift coefficient throughout the operational range of interest.

The selected operating condition corresponded to the region providing a favourable compromise between lift generation and drag penalty.

© 2026 IRJIET All Rights Reserved

ISSN (online): 2581-3048
Volume 10, Issue 6, pp 266-276, June-2026
https://doi.org/10.47001/IRJIET/2026.106034

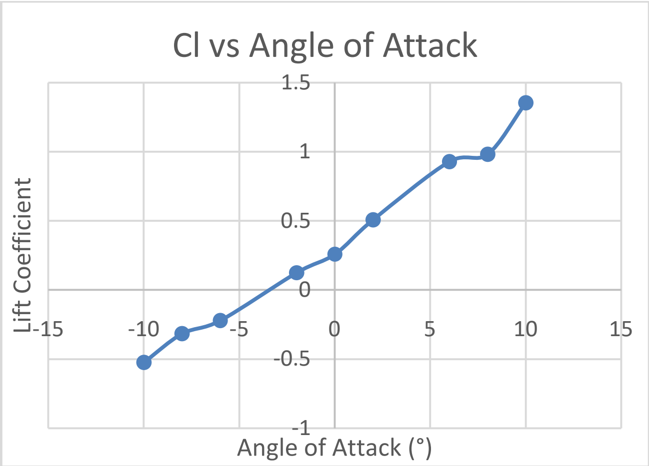

Figure 13: Variation of lift coefficient with angle of attack

10.2 Propeller Performance

The performance predictions obtained from Blade Element Theory and CFD are summarised in Table 2.

Table 2: Performance Comparison

Parameter	BET	CFD
Aquatic thrust (N)	293.46	296.70
Aquatic torque (N-m)	7.24	6.60
Aerial thrust (N)	20.10	15.40

To accurately maintain physical scaling principles congruent with the multimedium envelope, aquatic metrics were evaluated at the 1200 RPM baseline condition, whereas the aerial metrics reflect performance captured at the high-speed 8000 RPM flight profile.

The results exhibit excellent alignment in the dense aquatic medium, showing less than a 1.1% discrepancy in thrust. However, a noticeable variance is captured during high-speed aerial flight, where BET over predicts thrust by approximately 23.3% compared to the high-fidelity CFD model (20.10 N vs 15.40 N). This variation is physically driven by the severe rotational velocity of the 8000 RPM aerial cruise phase.

At this operating speed, complex 3D aerodynamic phenomena such as tip vortex generation, localized blade-to-blade wake interactions, and induction effects become highly pronounced. Because standard analytical Blade Element Theory assumes independent radial 2D flow sections, it fails to capture these highly non-linear 3D induced losses, thereby yielding a noticeably higher thrust approximation than the finite-volume Navier-Stokes domain.

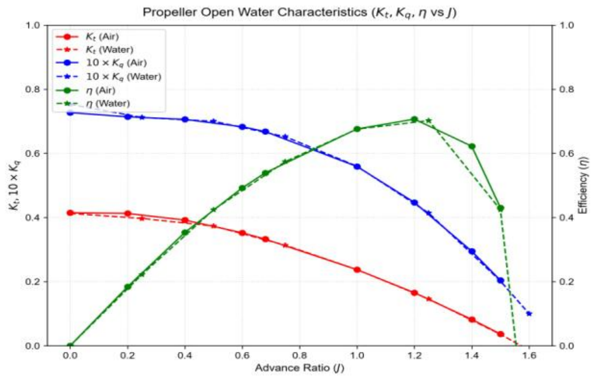

Figure 14: Non-dimensional propeller performance characteristics (Kt, Kq, η) versus advance ratio J for air and water operating conditions

To characterise performance beyond the single static operating point reported in Table 2, the propeller was additionally evaluated across a range of advance ratios (J) in both media. The resulting non-dimensional thrust coefficient (K_t), torque coefficient (K_q), and propulsive efficiency (η) curves are shown in Fig. 13.

Both media exhibit closely overlapping non-dimensional characteristics across most of the advance-ratio range, with peak efficiency of approximately 70% occurring near J ≈ 1.2 for air and J ≈ 1.25 for water, after which efficiency drops sharply as the propeller approaches the zero-thrust condition.

XI. FLOW FIELD ANALYSIS

The flow behaviour around the propeller was examined using pressure and velocity contour visualisations obtained from the CFD simulations. These visualisations provide qualitative insight into the aerodynamic and hydrodynamic mechanisms responsible for thrust generation.

11.1 Pressure Distribution

The pressure difference between the pressure side and suction side of the blade is the primary mechanism responsible for thrust production.

As expected, substantially larger pressure differences are observed during aquatic operation due to the significantly higher density of water. The pressure loading increases the generated thrust but also introduces considerably larger structural loads on the blade.

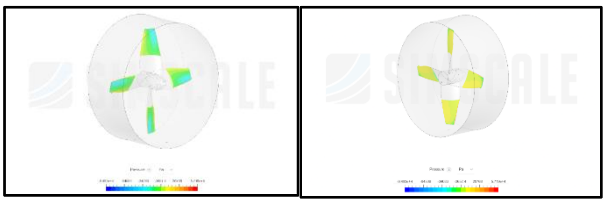

Figure 15: Pressure distribution around the propeller operating in water

© 2026 IRJIET All Rights Reserved

International Research Journal of Innovations in Engineering and Technology (IRJIET)

ISSN (online): 2581-3048

Volume 10, Issue 6, pp 266-276, June-2026

https://doi.org/10.47001/IRJIET/2026.106034

Figure 16: Pressure distribution around the propeller operating in air

11.2 Wake Characteristics

The velocity contours reveal the acceleration of fluid through the propeller disc and the formation of the downstream wake.

The wake generated in water remains coherent over a greater downstream distance compared to the aerial case. This behaviour is consistent with the increased momentum transfer associated with the higher fluid density.

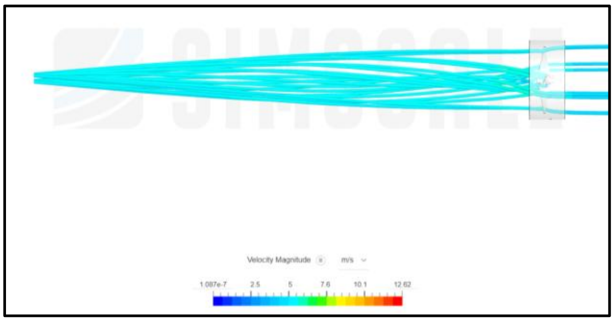

Figure 17: Wake structure generated by the propeller in water

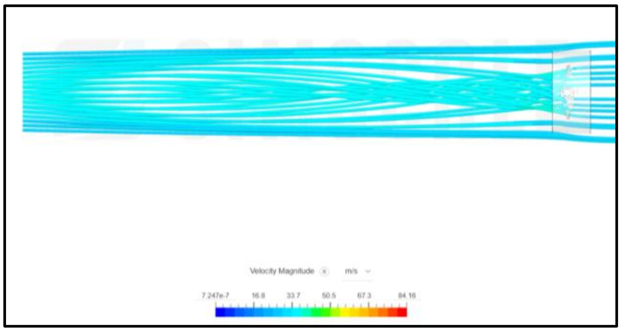

Figure 18: Wake structure generated by the propeller in air

XII. STRUCTURAL FEASIBILITY ASSESSMENT

An initial analytical structural assessment was conducted to estimate blade behavior under representative operating loads. The analysis considered bending loads, torsional loads, and centrifugal effects generated during rotation.

12.1 Material Selection

Polyamide 6 reinforced with 40% short carbon fibre (PA6CF40) was selected owing to its favourable stiffness-to-weight ratio, corrosion resistance, and compatibility with direct rapid prototyping extrusion methods. Extensively characterized by materials databases and composite engineering studies, shortfiber-reinforced thermoplastics provide a rigid structure capable of operating in dense marine flows without experiencing dramatic aeroelastic flutter or uncoupling [17], [18].

Table 3: Material Properties

Property	Value
Material	PA6-CF40
Tensile Strength	170 MPa
Young's Modulus	5 GPa
Density	1350 kg/m^3

12.2 Bending Stress

The thrust generated by the propeller produces a bending moment at the blade root. Assuming equal load sharing among the four blades:

$$F_b = \frac{293.46}{4} = 73.365\ \text{N} \quad \ldots\ldots\ldots(6)$$

$$M = F_b \times r_{eff} \quad \ldots\ldots\ldots(7)$$

where r_{eff} represents the effective moment arm of the distributed load along the span.

As a preliminary design check, the resulting bending stress was evaluated using classical beam theory at the blade root cross-section (width 0.05 m, thickness 0.006 m), giving a calculated bending stress of $\sigma_b \approx 9.8$ MPa. Under these first-order conservative approximations, the calculated value indicates analytical compliance with the allowable stress limit of the selected material.

12.3 Torsional Stress

The aerodynamic loading also produces a twisting moment on the blade, with an estimated torque of $T_b \approx 1.81$ N·m. The corresponding torsional stress was evaluated using standard torsion relationships, giving $\tau \approx 1.5$ MPa, substantially lower than the bending and centrifugal stress contributions.

12.4 Centrifugal Stress

The structural stress fields exhibit highly localized variations between the two operational configurations. During submerged water exploration (1200 RPM), the structural load profile is dominated by severe hydrodynamic pressure bending moments. Conversely, as the system transitions into the high-velocity aerial flight phase (8000 RPM), the operational angular velocity scales rapidly to:

© 2026 IRJIET All Rights Reserved

International Research Journal of Innovations in Engineering and Technology (IRJIET)

ISSN (online): 2581-3048

Volume 10, Issue 6, pp 266-276, June-2026

https://doi.org/10.47001/IRJIET/2026.106034

$$\omega = \frac{2\pi(8000)}{60} = 837.75 \text{ rad/s}..........(8)$$

The severe centrifugal stress resulting from this 8000 RPM aerial flight profile ($\sigma_c \approx 75.8$ MPa) introduces the single most significant tensile contribution encountered across the absolute mission lifetime, directly governing structural thickness limits at the blade root section.

12.5 Factor of Safety

Combining the bending and centrifugal stress contributions (the torsional contribution being comparatively negligible) gives a combined peak stress of $\sigma \approx 85.6$ MPa, which when compared against the 170 MPa tensile strength of PA6-CF40 yields a calculated analytical factor of safety of 1.92 under peak operating loads. This confirms that the blade geometry possess sufficient baseline strength for preliminary deployment while maintaining an optimized, lightweight structural profile.

XIII. BLADE DEFORMATION ESTIMATION

Although the calculated stress levels remain within allowable bounds, blade deformation can influence aerodynamic and hydrodynamic performance. To provide an initial approximation prior to experimental or detailed finite element validation, the blade was modeled analytically as an equivalent cantilever beam layout subjected to a continuous uniform spanwise distributed load assumption:

$$\delta = \frac{\omega L^4}{8EI}........................(9)$$

where ωdefines the equivalent hydrodynamic spanwise line load, L represents total blade length, E denotes the Young's Modulus of the selected PA6-CF40 material, and I serves as the area moment of inertia corresponding to the root cross-section geometry.

For a representative equivalent spanwise line load of w ≈ 917 N/m, the analytically estimated tip deflection was $\delta_{max} \approx$ 2.6 mm, corresponding to approximately 5% of the local chord length. This deformation is estimated to reduce the effective pitch angle by roughly 1.8° (shifting the operating angle of attack from approximately 6° to 4.2°), which in turn modifies the local angle of attack experienced by the blade sections and is associated with an estimated thrust reduction on the order of 14–18% relative to the undeformed blade. These deformation-related performance estimates are based on the analytical beam model and have not yet been confirmed against a coupled CFD–structural (FSI) simulation.

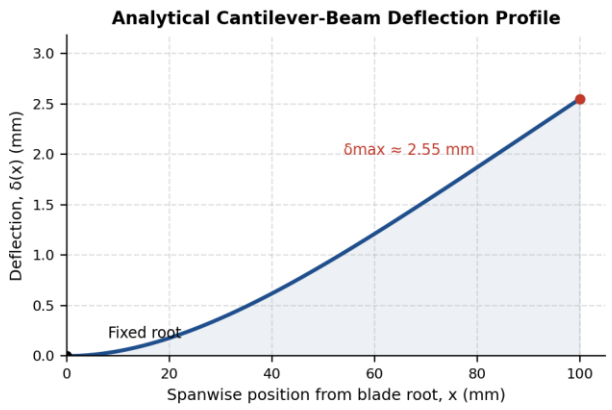

Figure 19: Illustration of blade deformation under loading

XIV. DISCUSSION

The results demonstrate that the proposed design methodology provides a practical framework for the development of dual-medium propellers.

The analytical predictions generated using Blade Element Theory showed reasonable agreement with the CFD results, particularly for aquatic operation. This indicates that BET can be effectively employed during preliminary design stages to establish blade geometry prior to higher-fidelity numerical assessment.

The CFD simulations revealed the expected differences between aerial and aquatic operation. Water generated significantly higher thrust levels due to its greater density, but this advantage was accompanied by increased torque requirements and larger structural loads.

The structural analysis showed that centrifugal effects dominate the stress distribution. While the selected material provides adequate strength, blade stiffness remains an important design consideration because excessive deformation can reduce propeller efficiency.

Overall, the study demonstrates that successful dualmedium propulsion requires a balance between aerodynamic performance, hydrodynamic performance, and structural integrity.

XV. SCOPE AND BOUNDARY CONDITIONS OF THE NUMERICAL MODEL

To systematically establish the baseline aerodynamic and hydrodynamic behavior of this dual-medium architecture, the physical domain was evaluated under a defined set of boundary conditions:

- A steady-state Moving Reference Frame (MRF) approach was purposefully chosen for the multi-fluid

© 2026 IRJIET All Rights Reserved

ISSN (online): 2581-3048
Volume 10, Issue 6, pp 266-276, June-2026
https://doi.org/10.47001/IRJIET/2026.106034

simulations under static bollard-pull conditions to isolate primary thrust generation fields.

- Transient cavitation boundaries and related multi-phase phenomena were kept outside the scope of this primary numerical characterization.
- One-way uncoupled analytical structural estimations were utilized to establish first-order structural boundaries prior to initiating full fluid–structure interaction (FSI) solvers.
- Structural calculations were bounded by classical beam and torsion theory to gauge core material limits rather than utilizing continuous local finite-element meshes.

Consequently, these outputs provide a verified, highly foundational numerical framework that maps out preliminary performance trends before entering the physical prototyping and manufacturing stages.

XVI. FUTURE WORK

Future work will focus on experimental validation and further optimisation of the proposed propeller design. Planned activities include:

- Fabrication of the propeller using additive manufacturing techniques.
- Static thrust testing in air.
- Static thrust testing in water.
- Measurement of thrust, torque, power consumption, and efficiency, following established thruster characterization methodologies [19].
- Cavitation assessment during underwater operation.
- Fluid–structure interaction studies.
- Geometry optimisation using advanced numerical techniques.

XVII. CONCLUSION

A systematic methodology for the design and numerical assessment of a dual-medium propeller has been presented. The development process combined Blade Element Theory, computational fluid dynamics, and structural evaluation to generate a propeller geometry capable of operating in both air and water.

The analytical and numerical results indicate that the proposed design can generate useful thrust in both operating environments while maintaining acceptable structural integrity. CFD simulations confirmed the expected flow behaviour and provided insight into pressure distribution, wake formation, and performance trends.

The structural assessment identified centrifugal loading as the dominant design consideration and highlighted the importance of maintaining adequate blade stiffness to minimise performance losses associated with deformation.

Although experimental validation remains necessary, the present work establishes a practical framework for future dual medium propeller development and optimisation.

ACKNOWLEDGMENT

The authors would like to thank the Department of Mechanical Engineering, AISSMS College of Engineering, Pune, for providing the facilities and support required for this work.

REFERENCES

[1] F. M. White, Fluid Mechanics, 9th ed., New York, NY, *USA: McGrawHill*, 2021.
[2] D. S. Drew, "Fluid-boundary transit mechanics for cross-domain robotic platforms," *IEEE Robotics and Automation Letters*, vol. 2, no. 4, pp. 2101–2108, Oct. 2017.
[3] R. Siddall and M. Kovac, "Submersible Unmanned Aerial Vehicles: Design challenges and state-of-the-art," *Robotics and Autonomous Systems*, vol. 62, no. 9, pp. 1350–1361, Sep. 2014.
[4] F. E. Weick, Aircraft Propeller Design, New York, NY, *USA: McGrawHill*, 1930.
[5] D. Lu, L. Zhou, and T. Wang, "Morphing and adaptive blade profiles for mixed-medium aquatic propulsion," *Journal of Fluids and Structures*, vol. 95, p. 102980, May 2020.
[6] X. Dang, Y. J. Jiang, and H. C. Chen, "Optimization design of a dual-medium propeller for hybrid aerial-underwater vehicles," *Ocean Engineering*, vol. 245, p. 110432, Feb. 2022.
[7] M. Maier and P. F. Schmidt, "Aerodynamic and structural boundaries of fixed-wing trans-media vehicle flight," *Aerospace Science and Technology*, vol. 112, p. 106612, May 2021.
[8] Mercado, E. J. Lopez, and C. R. Garcia, "Multirotor design constraints for sub-aerial atmospheric deployment," *Journal of Intelligent & Robotic Systems*, vol. 94, no. 2, pp. 411–427, Jun. 2019.
[9] O. Gur, "Aerofoil importance for propeller optimized design," *in Proceedings of the 56th 3AF International Conference on Applied Aerodynamics*, 2011, pp. 45–52.
[10] J. D. Anderson, Fundamentals of Aerodynamics, 6th ed., New York, NY, *USA: McGraw-Hill*, 2017.
[11] H. Glauert, "Airplane Propellers," in Aerodynamic Theory, W. F. Durand, Ed. Berlin, *Germany: Springer*, 1935, pp. 169–360.

ISSN (online): 2581-3048
Volume 10, Issue 6, pp 266-276, June-2026
https://doi.org/10.47001/IRJIET/2026.106034

[12] J. G. Leishman, Principles of Helicopter Aerodynamics, 2nd ed. New York, NY, *USA: Cambridge University Press*, 2006.

[13] H. K. Versteeg and W. Malalasekera, An Introduction to Computational Fluid Dynamics: The Finite Volume Method, *2nd ed., London, U.K.: Pearson*, 2007.

[14] F. R. Menter, "Two-equation eddy-viscosity turbulence models for engineering applications," *AIAA Journal*, vol. 32, no. 8, pp. 1598–1605, Aug. 1994.

[15] Y. Zhang, L. Zhou, and X. Wang, "Numerical investigation of propeller aerodynamic performance using overset mesh techniques," *Aerospace Science and Technology*, vol. 118, p. 106981, Nov. 2021.

[16] ANSYS Inc., *ANSYS Fluent Theory Guide*, Release 2021 R1, Canonsburg, PA, USA, 2021.

[17] F. C. Campbell, Structural Composite Materials, Materials Park, OH, *USA: ASM International*, 2010.

[18] Asahi Kasei Corp., Leona PA6-CF40 Technical Datasheet: Short Carbon Fiber Reinforced Structural Polyamide Properties, Tokyo, Japan, 2022.

[19] Laidani, M. S. Khan, and R. G. S. Johnston, "Development of a low cost thruster characterization test bench," *Journal of Marine Engineering & Technology*, vol. 19, no. 3, pp. 142–151, Jul. 2020.

Citation of this Article:

Hritika Chafekar, Prasad Gonewar, Karan Kunte, Dheeraj Kamble, & Dr. Sunil Patil. (2026). Design Methodology of a Dual-Medium Propeller Using BET. *International Research Journal of Innovations in Engineering and Technology - IRJIET*, 10(6), 266-276. Article DOI https://doi.org/10.47001/IRJIET/2026.106034

****

© 2026 IRJIET All Rights Reserved